Liquid-crystalline, liquid-ordered, rippled and gel lipid bilayer phases as observed with nile red fluorescence ☆

Jesús Sot [a], Leire Gartzia-Rivero [b], Jorge Bañuelos [b], Félix M. Goñi [a], Alicia Alonso [a,*]

[a] Instituto Biofisika (CSIC, UPV/EHU) and Departamento de Bioquímica, Universidad del País Vasco, 48940 Leioa, Spain
[b] Departamento de Química Física, Universidad del País Vasco, 48940 Leioa, Spain

ABSTRACT

The basic matrix of cellular membranes consists of a double layer (bilayer) of phospholipids. Semisynthetic lipid bilayers are commonly used in biophysical studies of membranes. According to temperature and composition, lipid bilayers can exist in liquid-crystalline (or liquid-disordered), liquid-ordered, rippled, and gel phases. In the present study, the hydrophobic, solvatochromic molecule Nile red has been used as a fluorescent probe to examine the physical state of bilayers of different compositions in the 15–60 °C range. Phospholipids with saturated or unsaturated acyl chains, in the presence or absence of cholesterol have been studied. Nile red shows absorption maxima at 520–550 nm and emission maxima at 580–640 nm, single photon excitation not being damaging to the system. A red/orange intensity ratio (ROIR) index has been used to normalize the results. ROIR varies clearly and reproducibly with the lipid phase, increasing in the order: liquid-ordered < gel < rippled < liquid-crystalline. It increases with temperature and decreases with cholesterol contents in the bilayers. Nile red allows an unusually clear observation of the rippled-to-liquid crystalline phase transition in saturated phospholipids. FLIM studies with Nile red also show differences between lamellar phases. Rotational relaxation times have been determined for Nile red in liquid-disordered (0.72 ± 0.010 ns), gel (1.16 ± 0.070 ns), and liquid-ordered (1.79 ± 0.14 ns) phases, the large value of the liquid-ordered phase being an indication of the sterol hindering probe tumbling in the hydrophobic matrix.

© 2022 The Authors. Published by Elsevier B.V. This is an open access article under the CC BY-NC-ND license (http://creativecommons.org/licenses/by-nc-nd/4.0/).

1. Introduction

The basic matrix on which cell membranes are built is a double layer, or bilayer, of lipids, usually glycerophospholipids in mammals [1,2]. The biophysical study of lipid bilayers has been enormously useful in understanding many properties of cell membranes [3]. When dispersed in water, phospholipids become organized in a number of mesophases, of which the lamellar phase is the most commonly found, and the one that reproduces most accurately the disposition of lipids in biomembranes [4,5]. Among glycerophospholipids, phosphatidylcholines (PC) appear most frequently in the cell membranes [6]. PC containing saturated fatty-acyl chains, when dispersed in water, can dopt different lamellar phases, depending on the composition and physical conditions (pressure, temperature) [4], among others: (i) the L_α (or L_d) is the liquid-crystalline, or liquid-disordered, phase, supposed to predominate in cell membranes, (ii) the L_β (or gel) phase occurs at a lower T than L_α, and in it the molecular motions of lipids are highly restricted, (iii) the $P_{\beta'}$, or rippled phase, occurs in a narrow temperature range, intermediate between the gel and fluid phases, (iv) finally the L_o, or liquid-ordered phase, is found only when the bilayers contain, in addition to saturated phospholipids, a high proportion of cholesterol, or similar sterols [7]. Sphingomyelin (SM) is a sphingolipid containing phosphorylcholine, i.e. the same polar group as PC. SM in aqueous media exists mostly in either the L_α or the $P_{\beta'}$ phases [8]. At variance with the saturated PC, the $P_{\beta'}$ phase of SM may predominate along a wide range of temperatures [8]. The L_β-to-L_α thermotropic phase transition, or, when a $P_{\beta'}$ phase exists, the $P_{\beta'}$ –to- L_α phase transition is often called the 'main transition', while the L_β-to- $P_{\beta'}$ phase transition is called the 'pre-transition'.

The structure of the different lipid phases was unraveled with the use of X-ray scattering [4]. Thermotropic phase transitions (e.g. L_β to $P_{\beta'}$, or $P_{\beta'}$ to L_α) were described using differential scanning calorimetry [9]. Fluorescence spectroscopy has found extensive application in the study of lipid phases. In this technique, the samples are doped with suitable fluorescent probes. To mention but a few examples, depolarization of diphenylhexatriene fluorescence

in the bilayer provides information on the phospholipid molecular order, thus it is commonly used in the detection of gel-fluid transitions [10]. Laurdan "generalized polarization" is also used in the detection of thermotropic transitions, two-photon excitation of this probe avoids the use of high-energy radiation that could damage the sample [11]. More recently, Niko et al. [12,13] have developed some push-pull pyrene derivatives, mainly PA and PK, whose photophysical properties are superior to those of Laurdan. PA and PK exhibit red-shifted absorption compatible with common diode laser (405 nm) excitation, bright fluorescence with large Stokes shift, and high photostability. Owing to its high sensitivity to environment polarity and hydration, the PA probe allowed the study of coexisting L_o and L_d phases in giant unilamellar vesicles (GUV) and demonstrated the difference in molecular order between plasma and cytoplasmic membranes in cells [13]. A recent contribution from this laboratory [14] expanded the previous data including parallel studies of PA and PK with GUV microscopy and multilamellar vesicle (MLV) spectroscopy, applying the Red/Blue Intensity Ratio (RBIR) as a general parameter for comparison, and calculating the appropriate microscopy-spectroscopy conversion coefficients,

Nile red (9-(diethylamino)-5H-benzo[α]phenoxazin-5-one), a fluorescent hydrophobic probe (Chart 1), was first used for the detection of neutral lipid deposits in tissue sections by Fowler and Greenspan [15–17]. It has since found a wide range of applications in cell biology, fluorescence microscopy and fluorescence spectroscopy [18,19], and, more recently, in the analysis of microplastics [20]. Nile red is also a source of solvatochromic derivatives that are increasingly applied to cell fluorescence microscopy [21,22]. The use of Nile red in the study of lipid bilayers has been, at best, limited. In the present contribution, we show the use of Nile red as a fluorescent probe in the study of phases and phase transitions in liquid and gel lipid bilayers. Nile red happens to be a useful reporter on the bilayer state, with which excitation can be used without noticeable photolytic effects [23].

2. Results

2.1. Fluorescence emission spectra of Nile red in lipid bilayers

The fluorescence emission spectra of Nile red (Fig. 1) were recorded in multilamellar vesicles composed of either DOPC, SM:Chol (70:30 mol ratio), or pure SM, at 0.4 mol% dye. These three compositions exist, in aqueous medium and at room temperature, in three different lamellar phases, respectively the liquid-
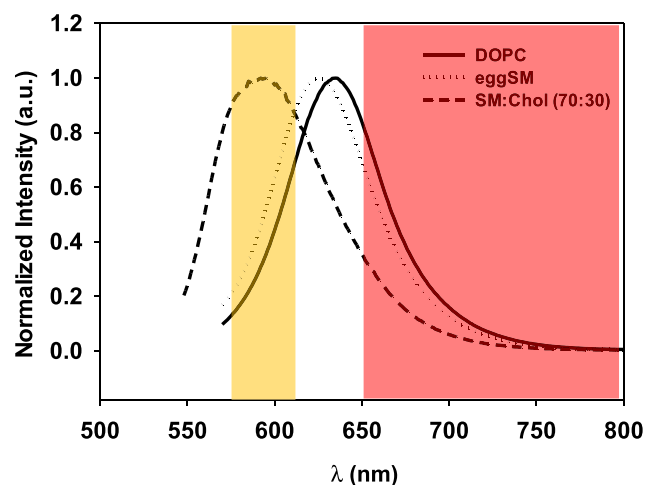
Fig. 1. Emission spectra of Nile Red. In DOPC (L_α phase), continuous line; in egg SM (L_β phase), dotted line; in SM:Chol (70:30) (L_o phase), dashed line. Spectra retrieved at 23 °C.

disordered (L_d), liquid-ordered (L_o) and gel phase (L_β). The maximum wavelengths of emission (λ_{em}) differ with the bilayer phase, decreasing in the order $L_d > L_\beta \gg L_o$. Wavelength data are summarized in Table 1, together with the corresponding emission – absorption spectral shifts, or Stokes shifts ($\Delta\nu$, in cm^{-1}). $\Delta\nu$ is a measure of the change in environmental polarity of the probe, thus Nile red appears to be in an environment whose polarity decreases in the order $L_d \geq L_\beta > L_o$. Note that the origin of the Nile red polarity-sensitive properties is ascribed to an intra-molecular electron transfer (ICT) process responsible for creating a charge transfer state, favorably stabilized in highly polar environments (Chart 1B) [24]. The emission energy from this state decreases when increasing the polarity, which would explain the redshift of the emission maximum in more polar environments.
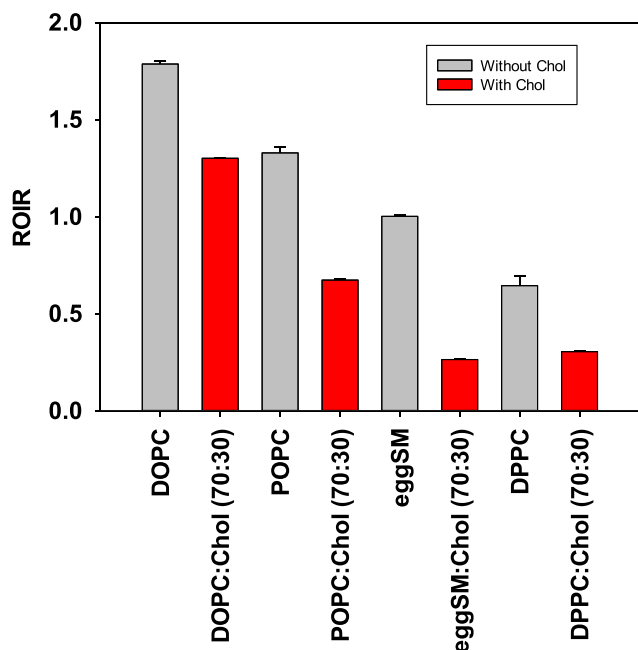
Further spectral data analysis was performed as in Sot et al. [14], using the ratiometric response of the dye, i.e. calculating the integral intensity ratio of red/orange regions of the emission band (573–613 nm/650–800 nm) (Fig. 1). The red/orange intensity ratio (ROIR) values of Nile red emission for a variety of bilayer compositions, some of them in Fig. 1, are shown in Fig. 2. The data in Fig. 2 include four couples of lipid compositions, one pure phospholipid and one phospholipid/Chol (70:30 mol ratio) mixture in
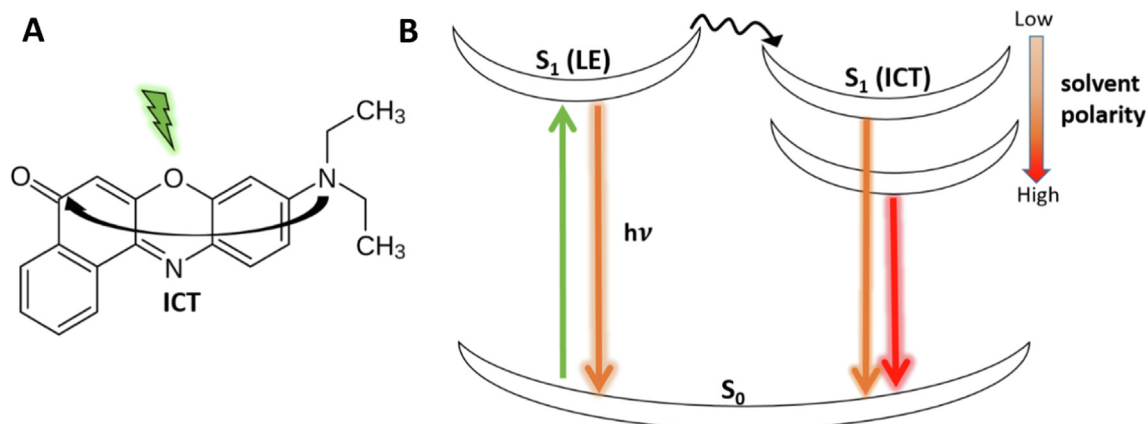
Chart 1. (A) Chemical structure of Nile Red showing the intramolecular charge-transfer (ICT) process from the electron donor diethylamino group towards the electron withdrawing aromatic system (into the carbonyl group). (B) Energy level diagram with emission from both, locally excited (LE) and intramolecular charge-transfer (ICT) states. The stabilization of the charge-transfer state is directly proportional to the polarity of the environment.

Table 1

Nile red spectral parameters. Effect of the different lipid phases. Measurements at 23 °C.

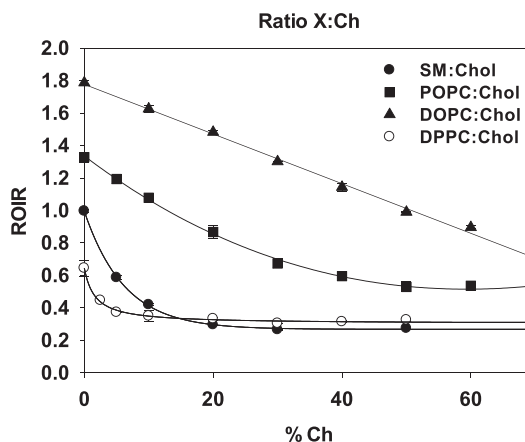| Sample (cm^{-1})	Phase	λ_{abs} (±1nm)	λ_{em} (±1nm)	$\Delta\nu$
DOPC	L_α	549	638	2547 ± 6
Egg SM:chol. (1:1)	L_o	523	592	2177 ± 6
Egg SM	L_β	544	630	2511 ± 6

Fig. 2. Red/Orange Intensity Ratio (ROIR) of Nile Red fluorescence emission in lipid bilayers of vrious compositions. Gray bars: pure phospholipids; red bars: phospholipids + 30 mol% cholesterol.

Fig. 3. Dose-dependent decrease of Nile red ROIR in phospholipid:cholesterol mixtures with increasing cholesterol concentrations. Average values ± S.D. (n = 3). The error bars are often smaller than the symbols.

each case. 30 mol% Chol is considered enough to generate a homogeneous L_o phase, at least with DPPC or SM [7,25].

The highest ROIR corresponded to L_d phases, DOPC > POPC (Fig. 2). Conversely, the lowest ROIR was associated to bilayers in the L_o phase, e.g. SM:Chol (70:30), or DPPC:Chol (70:30). On average, 30 mol% Chol decreased ROIR by 50.7 %. Bilayers in the L_β gel phase, such as SM or DPPC gave lower ROIR values than those in the L_d phase (Fig. 2). In view of the results showing that the probe is sensitive to membrane order/rigidity, and in particular to the presence of L_o phases, Nile red could be used to distinguish between the three main types of lamellar phases.

The effect of Chol on Nile red ROIR was studied in more detail, examining phospholipid bilayer samples in which Chol concentration was varied between 0 and 50–66 mol% (Fig. 3). The maximum Chol concentration was limited by the solubility of the sterol in the corresponding phospholipid [26]. In all samples ROIR decreased monotonically with Chol concentration. In bilayers formed by DPPC or SM, essentially saturated phospholipids that are known to give rise to L_o phases in the presence of sterols [7,27,28], ROIR decreased rapidly for Chol concentrations in the 0–10 mol% interval, then kept a constant value at $\geq$ 20 mol%. With POPC mixtures the decrease exhibited a lower slope, and ROIR remained stable only at $\geq$ 50 mol% Chol. Finally, in the case of the more unsaturated DOPC, not known to give rise to L_o phases with Chol, ROIR decreases linearly with Chol concentration between at least 0 and 60 mol%. Thus L_o phases can be characterized with Nile red by a ROIR < 0.5.

Nile red ROIR was then examined as a function of temperature (Fig. 4). This is relevant, among other reasons, because saturated

phospholipids are known to undergo thermotropic phase transitions from gel (L_β) to fluid (L_d), or, in some cases, from rippled ($P_{\beta'}$) to fluid. Four kinds of lipid compositions were tested: (a) pure phospholipids like DOPC or POPC, that remain in the L_d phase throughout the T interval in our study (15–60 °C), (b) DPPC, that exhibits two thermotropic transitions, from L_β to $P_{\beta'}$ near 30 °C, and from $P_{\beta'}$ to L_d at about 41 °C, (c) egg SM, with a single thermotropic transition from $P_{\beta'}$ to L_d at about 40 °C, and (d) the equimolar mixtures DPPC:Chol and egg SM:Chol, that remain in the L_o phase at least between 15 and 60 °C [3]. DOPC and POPC remain along the tested T interval in the 1.5–2 region of ROIR. The equimolar phospholipid:Chol mixtures give rise to ROIR values near or below 0.5, indicating L_o phase behavior at all temperatures.

The comparative behavior of DPPC and egg SM is more interesting (Fig. 4B), because in DPPC bilayers Nile red ROIR marks clearly the gel (L_β) to rippled ($P_{\beta'}$) phase transition near 30 °C, as an increase from $\approx$0.65 to $\approx$0.85, then the $P_{\beta'}$ to L_d transition as an abrupt change in slope near 40 °C. Correspondingly, in egg SM membranes, the rippled $P_{\beta'}$ to fluid L_d transition is equally indicated by a change in slope at $\approx$40 °C. This may be relevant to the use of Nile red because, to the authors' knowledge, no other fluorescent procedure can detect the $P_{\beta'}$ to L_d transition with such a simple instrument (single-photon, standard spectrofluorometer), and a very straightforward data treatment.

2.2. Nile red in FLIM studies

Nile red sensitivity to lipid bilayer phases suggested that it could also be useful in fluorescence lifetime imaging microscopy (FLIM). This was confirmed in experiments as shown in Fig. 5. Giant unilamellar vesicles (GUV) were prepared by an electroformation procedure and examined under a two photon excitation fluorescence microscope. GUV of the compositions described in Fig. 4A were studied. FLIM images of the various GUV preparations are shown in Fig. 5A-F, together with the corresponding histograms of lifetimes (tau), and average tau ± SD. Average tau values are comparatively shown in Fig. 5G, as a bar graph. They are lowest
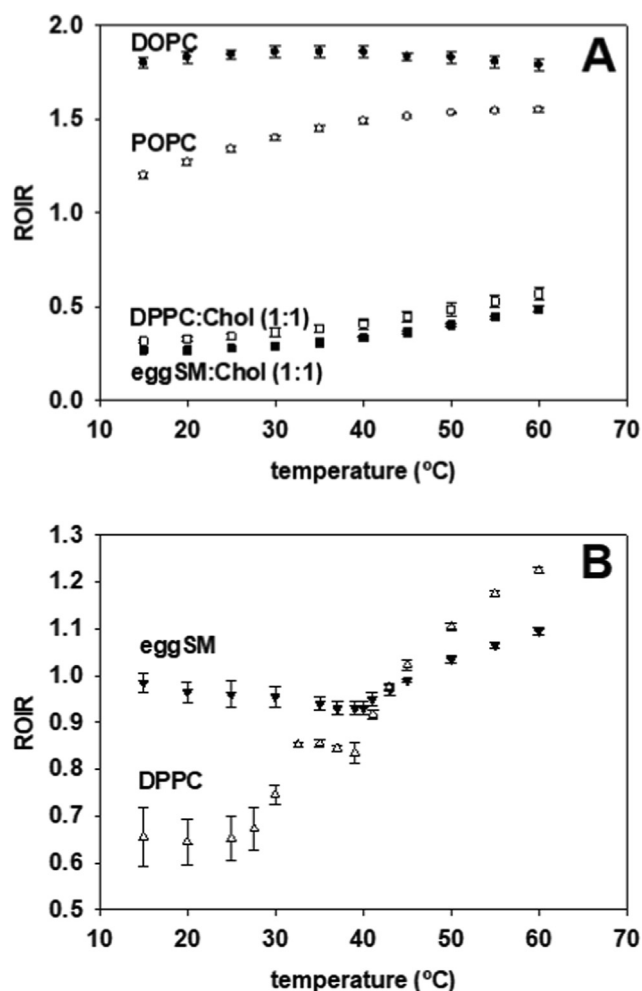
Fig. 4. Temperature effects on Nile red ROIR. (A) Bilayers composed of DOPC, POPC, DPPC:Chol (1:1), eggSM:Chol (1:1). (B) Data obtained with eggSM, DPPC. Average values ± S.D. (n = 3). The error bars are often smaller than the symbols.

(around 3 ns) for the fluid bilayers, highest (around 5 ns) for those in the L$_o$ state, and intermediate for the L$_\beta$ gel phase, thus again Nile red exhibits its capacity to report on the physical state of lipid bilayers. Note that, for the L$_\beta$ gel bilayers, a heterogeneity is clearly detected in the GUV, with yellow and red regions. Such heterogeneity is reflected in a wide range of tau values, in turn leading to higher SD values for these gel bilayer preparations. This might be reflecting that, under the conditions of the experiment, part of the lipids are undergoing a thermotropic gel-fluid transition. Both DPPC and eSM have calorimetric transitions centered around 40 °C (see above), thus at the room T at which the FLIM measurements are performed the respective systems should be well below the transition T. However, the possibilities that laser illumination causes local heating in the sample holder, or even that the thermal behavior of GUV in an essentially 2-dimensional medium is different from that of MLV in suspension (as used in the calorimetric experiments), cannot be excluded. Thus, Nile red FLIM offers the advantage, over the standard fluorescence measurements in cuvettes, to reveal microheterogeneities in the membranes under study.

2.3. Nile red fluorescence relaxation times in lipid bilayers

Fluorescence signal of a chromophore is a powerful tool to explore the polarity and dynamics of its environment. In this sense,

time-dependent fluorescent shift (TDFS) measurements enable monitoring the mobility and transversal gradients of hydration in lipid bilayers. Upon excitation of a fluorophore, its dipolar moment changes ultra-rapidly and the solvation shell must respond to it immediately. The subsequent dipolar relaxation process is more difficult when probe motion is hindered. Thus, the average relaxation time (τ_r) is directly related to the viscosity of the probe environment (i.e., reorientational motions of the solvent molecules). The relaxation time enables the numerical determination of the solvation kinetics and was obtained integrating the spectral response function, *C(t)*:

$$\tau_r = \int_0^\infty C(t)dt \tag{1}$$

where $C(t) = \dfrac{v(t) - v(\infty)}{v(0) - v(\infty)} = \dfrac{v(t) - v(\infty)}{\Delta v}$ (2)

Δv is the Stokes shift (Table 1), equal to the difference between energies of the Frank-Condon and the fully relaxed state, $v(\infty)$, whereas $v(t)$ is the emission maximum at each specific time. TDFS of the peak maxima, $v(t)$, was determined via time-resolved emission spectra (TRES) measurements. For each sample, spectrally resolved fluorescence decays (Fig. 6) were recorded along the emission window (orange-red) of the Nile Red (in 5-nm steps). Note that the measurements on the blue edge of the emission spectrum give rise to multiexponential decays (see the shape of the curve for shorter wavelengths in Fig. 6), inherent to the dual contribution from both the LE (locally excited) state, with a short fluorescence lifetime, and the ICT state, with a longer fluorescence lifetime. However, as the emission wavelength increases the contribution of the shorter lifetime LE state becomes progressively weaker, and on the red edge (∼640 nm) the longer lifetime ascribed to the ICT state turns predominant. From these set of fluorescence decays, normalized emission spectra were later reconstructed as a function of time (Fig. 7). Thus, a $v(t)$, or emission maximum at time t, was obtained from each spectrum. $v(t)$ values could then be introduced in the C(t) equation, and C(t) function was finally plotted versus time (Fig. 8).

The integrated rotational relaxation times τ_r were obtained from the areas below the curves in Fig. 8. τ_r values increased in the order L$_d$ (0.72 ± 0.010 ns), gel (1.16 ± 0.070 ns), and L$_o$ (1.79 ± 0.14 ns). In general, higher τ_r values are an indication of a higher microviscosity (lower fluidity). However the higher τ_r value of L$_o$ with respect to gel phases is probably an indication of cholesterol hindering probe motion, and of specific H bonds between the cholesterol hydroxyl group and the accessible electron pair from the Nile Red amino group, rather than of an overall low fluidity in L$_o$ samples. Moreover, the already mentioned specific interactions between probe and cholesterol would imply the amino lone pair to be less accessible to participate in the intramolecular charge-transfer (ICT) process. This would lead to an excited state with a decreased polar character, and hence, a smaller shift of the emission spectrum, as shown for the L$_o$ sample, with the lowest Stokes shift (Δv) value.

3. Discussion

Nile red is an easily available chemical, with minimal or low hazard rates, unless chronically administered (Chemwatch Hazard Ratings, https://datasheets.scbt.com/sc-203747.pdf). Biological applications normally require the use of ≥ 97.0 % purity product, even so the price is in the range of other biological dyes. Its absorption and emission ranges (respectively 520–550 nm and 580–640 nm) allow single-photon excitation without significant photolysis. Until now, its use in Biology has been mainly in the staining of
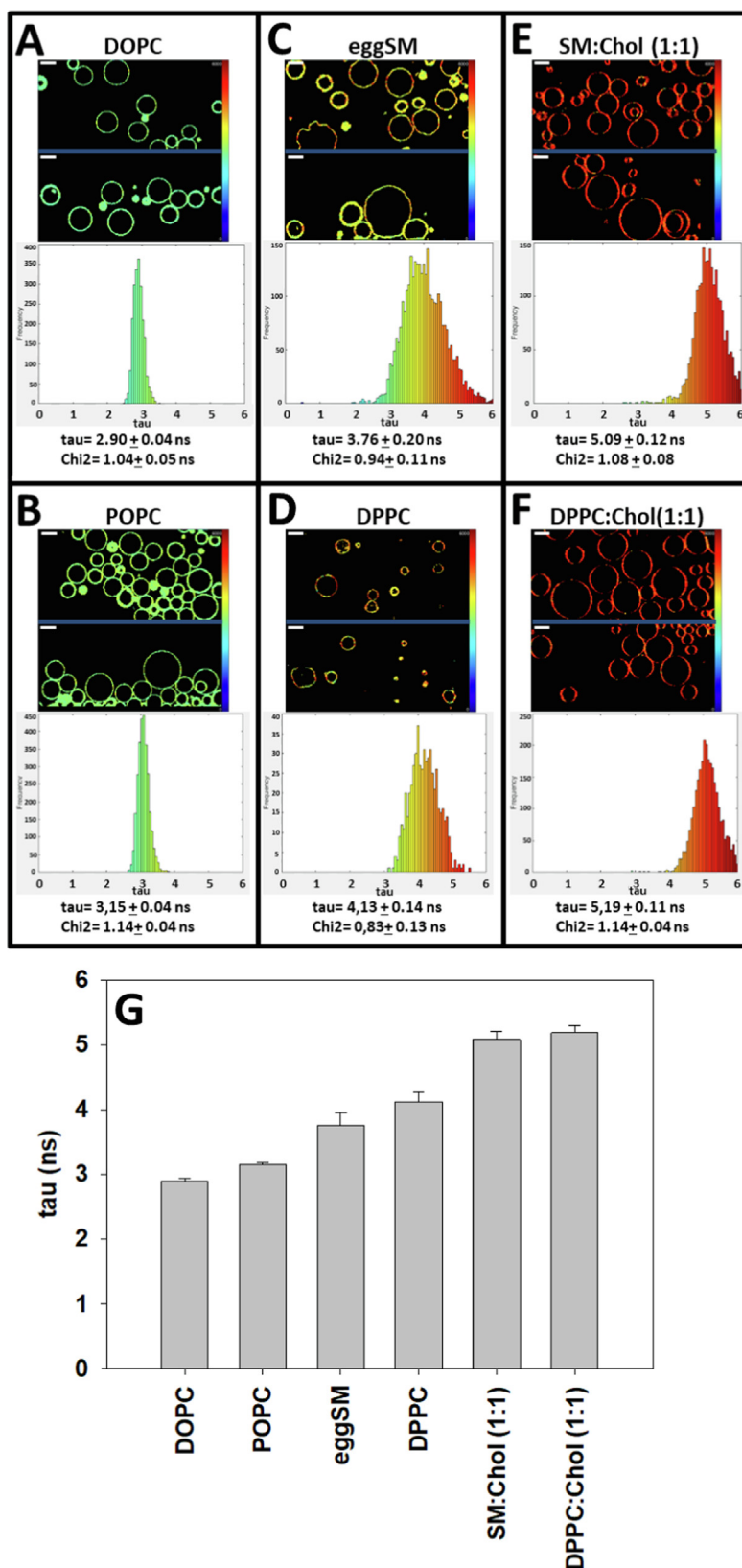
Fig. 5. FLIM of Nile Red in giant unilamellar vesicles (GUV). Effect of different lipid phases. FLIM-images (A-F, average lifetimes) with their corresponding fluorescence lifetime histograms: (A,B) DOPC and POPC, bilayers in the L_α phase. (C,D) Egg SM and DPPC, bilayers in the L_β phase. (E,F) SM:Chol (1:1) and DPPC:Chol (1:1), bilayers in the L_o phase. Scale bar: 20 μm. (G) Average fluorescence lifetimes (tau) of Nile red fluorescence. Average values ± S.D. (n = 20).

lipid droplets in thin tissue sections for microscopy [15–17], and only recently its solvatochromic properties have been taken into account. Solvatochromic dyes are fluorescent probes with the ability to identify the lipid organization of biomembranes in live cells
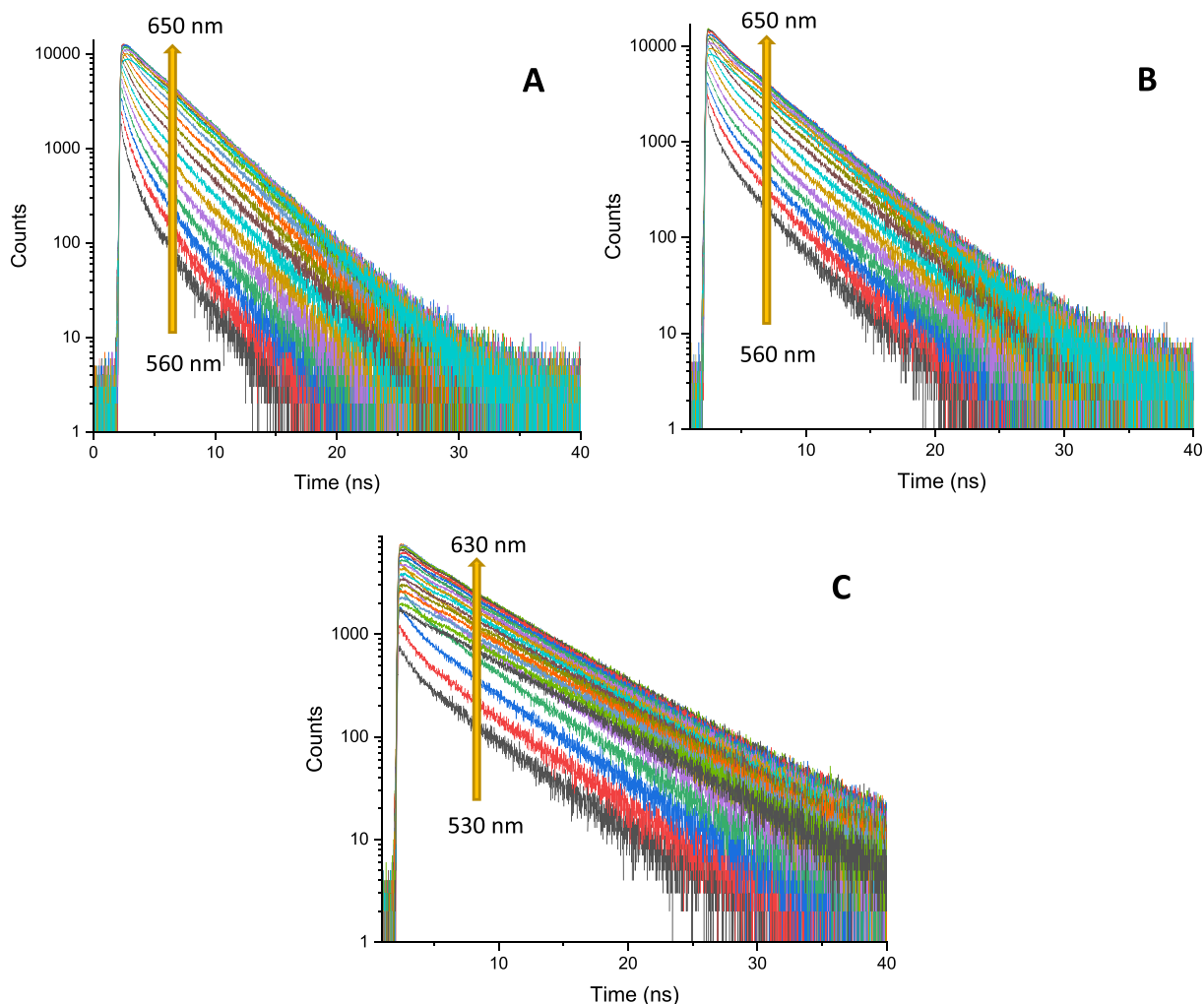
Fig. 6. Spectrally resolved fluorescence decays for Nile Red in lipid bilayers. (A) DOPC, L_α, excitation at 550 nm, emission in the 560–650 nm interval, 5 nm steps. (B) Egg SM, L_β, excitation at 550 nm, emission in the 560–650 nm interval, 5 nm steps. (C) Egg SM:cholesterol (1:1), L_o, excitation at 510 nm, emission in the 530–630 nm interval, 5 nm steps.

by changing the color of their fluorescence. They have been applied to monitor the lipid order of biomembranes in live cells [19]. In the present paper, Nile red has been used as a solvatochromic dye in lipid bilayers (liposomes) of known composition, and whose physical properties are also known, in order to establish a correlation between membrane properties and Nile red fluorescence emission. Fluorescence spectroscopy observations (in cuvette rather than in a microscope), have been performed in order to obtain overall data from a large number of vesicles in a largely isotropic medium.

The main observations in this paper are (i) the Nile red capacity to shift its fluorescence emission, or its red/orange intensity ratio (ROIR) values, with the different lamellar phases (Fig. 2,3), (ii) its applicability to FLIM observations to differentiate lamellar phases (Fig. 5), and (iii) its suitability for the study of the correlation between physical state of the bilayer and fluorescence emission relaxation times (Fig. 8). Previous studies by Danylchuk et al. [21] had shown the capacity of Nile red to distinguish between the L_o and L_d phases. Many fluorescent dyes are known that respond to changes in lipid phase properties, from this point of view Nile red is not particularly useful. Nevertheless, the fact that ROIR values, presumed to decrease with decreasing bilayer fluidities (see e.g. Fig. 2, gray bars), become actually lower in the presence of cholesterol (compare gray and red bars in Fig. 2) would constitute an anomaly, because cholesterol, at the 30 mol% ratios

used in the experiments in Fig. 2, would decrease the fluidity of the originally fluid bilayers, in the L_α phase, but it would increase the fluidity of the bilayers in the L_β or gel phase, inducing formation of the liquid-ordered L_o phase [7,9]. Thus there is no linear correlation between Nile red ROIR and bilayer fluidity. A reasonable explanation for the observed anomaly would be that the probe is actually reporting on its capacity to diffuse in the membrane matrix. In general, an increased fluidity, when it arises from an increased fatty acid unsaturation, or an increased temperature, will facilitate probe diffusion, and ROIR will also increase. However, when the increased fluidity arises from the introduction of cholesterol in an originally L_β or gel bilayer, the rigid, flat sterol molecule perturbs the quasi-crystalline organization of the fatty acyl chains thus increasing the overall fluidity of the bilayer, i.e. the lateral diffusion coefficient of lipids increases, while the probe motion is restricted by the sterol in the hydrophobic bilayer matrix, and ROIR decreases. Nile red is a very hydrophobic molecule (see Chart 1), at variance with phospholipids and cholesterol it is unlikely to be oriented along the bilayer polarity axis, thus the sterol-caused increase in molecular order in the L_o phase is not compensated by an increased lateral diffusion.

A rather unique property of Nile red is its capacity to distinguish between the rippled $P_{\beta'}$ and the L_β or L_α phases, and to monitor the $P_{\beta'}$ to L_α thermotropic transitions, as shown in Fig. 4B. In DPPC the
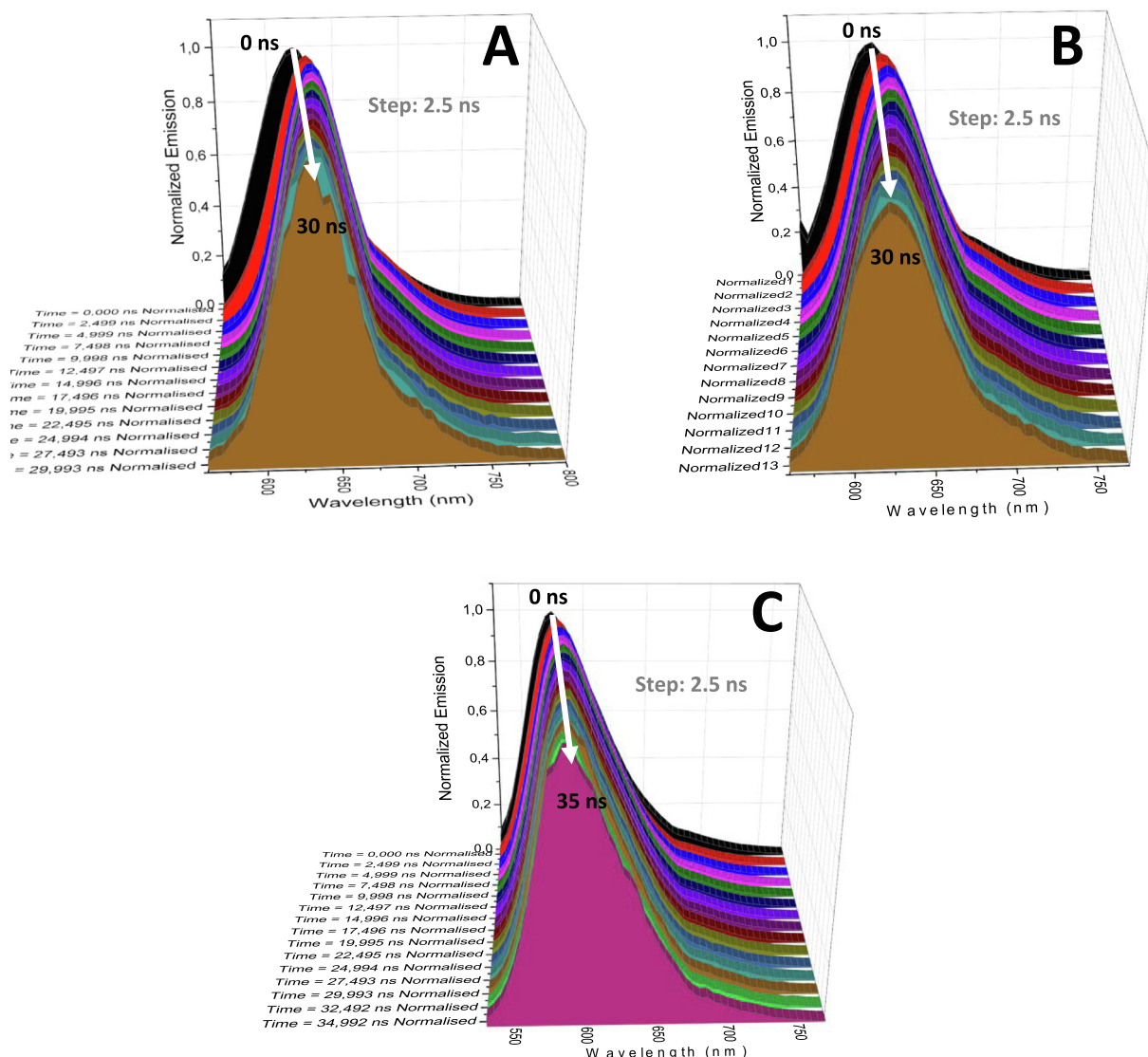
Fig. 7. Time-resolved emission spectra for Nile Red in lipid bilayers. Times vary between 0 and 30–35 ns, in 2.5 ns steps. Samples as indicated in Fig. 6. Emission maxima at each time are designated ν (t).

ripple phase exists between ≈33–41 °C [29], while in egg SM it extends for at least 30 °C below the 'main transition' to liquid-crystalline at 40 °C [8]. For both DPPC and egg SM, Nile red ROIR has a value of about 0.9 for the $P_{\beta'}$, which increases sharply above 40 °C. Below the 'main transition' temperature, ROIR decreases rapidly with temperature for DPPC, indicating the ripple-to-gel transition, but remains virtually constant for egg SM in the same temperature range, along which this lipid remains in the rippled $P_{\beta'}$ phase.

With respect to Nile red applicability to FLIM measurements that allow distinguishing between lamellar phases, is should be noted that FLIM is an imaging technique, the images originating from a two-photon fluorescence microscope. The fact that Nile red can be used to analyze the molecular order of individual bilayers (Fig. 5) adds a new dimension to its above discussed applicability to measurements in cuvette. Levitt et al. [30] had applied Nile red to the confocal microscopy of HeLa cells, showing that fluorescence lifetime is a viable contrast parameter for distinguishing lipid droplets from other stained lipid-rich regions. Our study with lipid bilayers of defined compositions is a demonstration of the

capacity of this dye to measure lipid order in isolated membranes, through FLIM.

Finally Nile red is a suitable fluorescent molecule for the convenient measurement of fluorescence rotational relaxation times, with excitation/emission maxima (when in lipid bilayers) around 520/640 nm, depending on the lipid phase (Table 1). Thus the fluorescence emission spectra can be used to retrieve relaxation time data. Relaxation time is a parameter describing the time-dependence of the tumbling of a molecular entity in a medium of viscosity η as originally defined by Debye, and used by Perrin in the original development of the theories of rotational motion of fluorophores [31,32]. Molecules exhibiting several rotational degrees of freedom will markedly decrease fluorescence intensity, thus the relationship between relaxation times and fluorescence emission (Fig. 6-8). The different relaxation times observed for Nile red in the different bilayers (Fig. 8) show the relationship between bilayer lipid order and probe relaxation times. The higher relaxation times in the L_o state are clearly related to the hindering of probe molecular tumbling by the rigid cholesterol molecules, and could be one of the reasons why the Nile red probe is able to differentiate between the L_β and L_o phases, as discussed above. Another
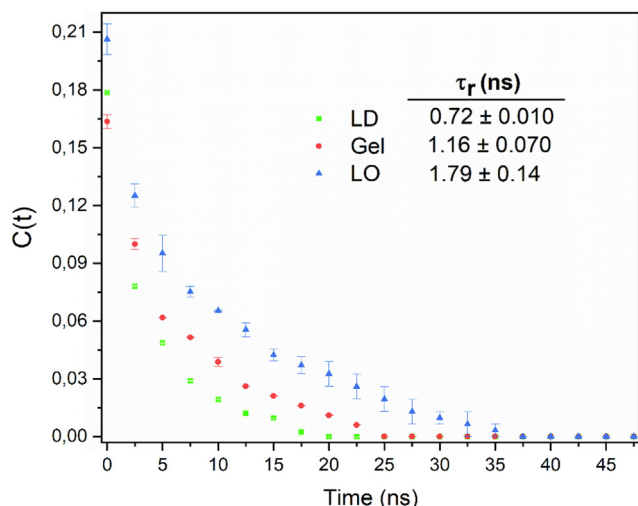
Fig. 8. Mean integrated relaxation times of Nile Red. Correlation function, C(t), for spectral relaxation of Nile Red [eq. (2)]. Relaxation times τ_r are obtained by integration of the C(t) vs time curves. Samples as indicated in Fig. 6. A longer τ_r indicates that the probe tumbling is more hindered.

reason could be the polarity surrounding the probe, which is directly related to the Stokes shift. When the polarity surrounding the probe decreases, the Stokes displacement decreases. As shown in Table 1, the Stokes shift in the L_o-phase membranes is lower than in the L_β-phase membranes, indicating that, in the L_o-phase membranes the probe is in a less polar environment. This would agree with the experiments by Cheng et al. [33] who observed that the increase of cholesterol in lipid membranes increased the hydration of the membrane exterior and decreased the hydration of the inner part of the membrane, or what is the same, it decreases the polarity of the membrane core. Considering the hydrophobicity of Nile red, it should be found in the inner membrane core, and this would explain the Stokes shift of Nile red in L_o phases.

4. Materials and methods

4.1. Materials

Dioleoyl phosphatidylcholine (DOPC), 1-palmitoyl-2-oleoyl-*glycero*-3-phosphocholine (POPC), dipalmitoyl phosphatidylcholine (DPPC), egg sphingomyelin (SM) and cholesterol (Chol) were purchased from Avanti Polar Lipids (Alabaster, AL). Nile red was purchased from Sigma.

4.2. Multilamellar vesicles (MLV)

Stocks of pure lipids and probes were prepared dissolved in a solution of chloroform/methanol (2:1 v/v) and stored at −20 °C. Multilamellar vesicles (MLV) for spectrofluorometric assays were prepared by mixing the desired lipids and Nile Red at a 250:1 (lipid:Nile red) ratio and evaporating the organic solvent under a stream of nitrogen. The sample was then kept under high vacuum for 90 min to remove any residual solvent. The resulting lipid film was hydrated by addition of the buffer solution (HEPES 25 mM, 150 mM NaCl, EDTA 1 mM, pH 7.4) at a temperature above the lipid main phase transition temperature, followed by vigorous vortex mixing. Finally, the samples were sonicated in a bath sonicator FB-15049 (Fisher Scientific, Waltham, USA) at a temperature above the transition temperature for 10 min.

4.3. Giant unilamellar vesicles (GUVs)

Giant unilamellar vesicles (GUV) were prepared by electroformation method first developed by Angelova and Dimitrov [34,35]. GUVs were formed in a PRETGUV 3 chamber supplied by Industrias Técnicas ITC (Bilbao, Spain), that allows direct visualization under the microscope, as described in [36]. Stock solutions of lipid mixtures under study were to a final concentration of 0.2 mM in chloroform/methanol (2:1 v/v). 3 µl of the desired stock solution were added to the surface of platinum electrodes and solvent traces were removed by evacuating the chamber under high vacuum for at least 90 min. The Pt electrodes were covered with 500 µl of 300 mM sucrose preheated at 60 °C The Pt wires were connected to an electric wave generator (TG330 function generator, Thurlby Thandar Instruments, Huntington, UK) under AC field conditions (10 Hz, 0.9 V) for 2 h at 60 °C. Finally, added 0.08uM Nile Red in DMSO and leave to equilibrate, in the absence of light, overnight.

4.4. Fluorescence spectroscopy

1 mM MLV containing Nile red were prepared. Then, the samples were diluted to a 0.3 mM lipid concentration and the fluorescence spectra of the Nile Red probe was measured in a QuantaMaster 40 spectrofluorometer (Photon Technology International, Lawrenceville, NJ). Emission spectra were collected between 570 and 800 nm, exciting at 540 nm. A thermal TC125 controller (Quantum Northwest, Liberty Lake, USA) was used to stabilize the sample temperature at 23 °C, unless otherwise stated. Once the emission spectra were obtained, in order to calculate the Red/Orange Intensity Ratio (ROIR), the areas of the orange (573–613 nm) and red (650–800 nm) regions were subtracted with the software PTI Felix-GT software (Photon Technology International, Lawrenceville, NJ).

4.5. Fluorescence lifetime imaging (FLIM)

FLIM was performed at the The Basque Resource for Advanced Light Microscopy (BRALM), Instituto Biofisika. Lifetime images were acquired on a Leica TCS SP5 microscope through a $63\times/1.30$ water objective (Leica). The samples were excited at 1020 nm using a 100-fs pulsed laser (Mai-Rai HP DS: Spectra Physics), specifically optimized for use in multiphoton microscopy. Time-resolved fluorescence detection was performed in the 581–653 nm range using a hybrid detector (HyD RLD, Leica Microsystems CMS GmbH, Germany). Lifetime imaging was carried out with a TCSPC system (SPC-830, Becker & Hickl, Germany). Image processing was performed using the FLIMfit software tool developed at Imperial College London and TRI2 (Paul R. Barber, University of Oxford).

4.6. Time-resolved fluorescence spectroscopy

Spectrally resolved decay curves of DOPC (L_α phase), egg SM (L_β phase) and SM:Chol (70:30) (L_o phase) samples were recorded using a Edinburgh Instruments spectrofluorimeter (model FLSP920) using time-correlated single-photon counting (TC-SPC). Decay curves were recorded as a function of the emission wavelength in the 560–800 nm range (5-nm wavelength increments) for a fixed recording time (180 s per wavelength) by means of a microchannel plate detector (Hamamatsu C4878) of picosecond time-resolution (20 ps). Samples were measured in 1 cm path-length quartz cuvettes, with excitation from a wavelength-tunable Fianium Supercontinuum laser (10 MHz repetition rate) at 510 nm (for L_o) and 550 nm (L_α and L_β). The emission spectra at different times after excitation were obtained by averaging the

integrated fluorescence intensity for different time windows in the nanosecond time intervals (2.5 ns) after the excitation pulse (between 0 and 35 ns).

Data availability

Data will be made available on request.

Declaration of Competing Interest

The authors declare that they have no known competing financial interests or personal relationships that could have appeared to influence the work reported in this paper.

Acknowledgments

References

[1] S.J. Singer, G.L. Nicolson, The fluid mosaic model of the structure of cell membranes, Science 175 (4023) (1972) 720–731.

[2] F.M. Goñi, The basic structure and dynamics of cell membranes: an update of the Singer-Nicolson model, BBA 2014 (1838) 1467–1476.

[3] D. Marsh, Handbook of Lipid Bilayers, CRC Press, Boca Raton FA, US, 2013, p. 1174.

[4] V. Luzzati, X-ray diffraction studies of lipid-water systems, in: D. Chapman (Ed.), Biological Membranes, Academic, New York, 1968, pp. 71–123.

[5] A.D. Bangham, M.M. Standish, J.C. Watkins, Diffusion of univalent ions across the lamellae of swollen phospholipids, J. Mol. Biol. 13 (1) (1965) 238–IN27.

[6] G. van Meer, D.R. Voelker, G.W. Feigenson, Membrane lipids: where they are and how they behave, Nat. Rev. Mol. Cell Biol. 9 (2008) 112–124.

[7] J.H. Ipsen, G. Karlström, O.G. Mouritsen, H. Wennerström, M.J. Zuckermann, Phase equilibria in the phosphatidylcholine-cholesterol system, BBA 905 (1987) 162–172.

[8] Z. Arsov, E.J. González-Ramírez, F.M. Goñi, S. Tristram-Nagle, J.F. Nagle, Phase behavior of palmitoyl and egg sphingomyelin, Chem. Phys. Lipids 213 (2018) 102–110.

[9] D. Chapman, Phase transitions and fluidity characteristics of lipids and cell membranes, Q. Rev. Biophys. 8 (2) (1975) 185–235.

[10] M. Shinitzky, Y. Barenholz, Fluidity parameters of lipid regions determined by fluorescence polarization, BBA 515 (4) (1978) 367–394.

[11] G. Gunther, L. Malacrida, D.M. Jameson, E. Gratton, S.A. Sánchez, Laurdan since Weber: The Quest for Visualizing Membrane Heterogeneity, Acc. Chem. Res. 54 (2021) 976–987.

[12] Y. Niko, S. Kawauchi, G.-I. Konishi, Solvatochromic pyrene analogues of Prodan exhibiting extremely high fluorescence quantum yields in apolar and polar solvents, Chemistry. 19 (30) (2013) 9760–9765.

[13] Y. Niko, P. Didier, Y. Mely, G. Konishi, A.S. Klymchenko, Bright and photostable push-pull pyrene dye visualizes lipid order variation between plasma and intracellular membranes, Sci. Rep. 6 (2016) 18870.

[14] J. Sot, I. Esnal, B.G. Monasterio, R. León-Irra, Y. Niko, F.M. Goñi, A. Klymchenko, A. Alonso, Phase-selective staining of model and cell membranes, lipid droplets and lipoproteins with fluorescent solvatochromic pyrene probes, Biochim. Biophys. Acta, Biomembr. 1863 (2021) 183470.

[15] P. Greenspan, E.P. Mayer, S.D. Fowler, Nile red: a selective fluorescent stain for intracellular lipid droplets, J. Cell Biol. 100 (1985) 965–973.

[16] P. Greenspan, S.D. Fowler, Spectrofluorometric studies of the lipid probe, nile red, J. Lipid Res. 26 (7) (1985) 781–789.

[17] S.D. Fowler, P. Greenspan, Application of Nile red, a fluorescent hydrophobic probe, for the detection of neutral lipid deposits in tissue sections: comparison with oil red O, J. Histochem. Cytochem. 33 (8) (1985) 833–836.

[18] Y. Zhao, W. Shi, X. Li, H. Ma, Recent advances in fluorescent probes for lipid droplets, Chem. Commun. (Camb.) 58 (10) (2022) 1495–1509.

[19] Y. Niko, A.S. Klymchenko, Emerging solvatochromic push-pull dyes for monitoring the lipid order of biomembranes in live cells, J. Biochem. 170 (2021) 163–174.

[20] V.C. Shruti, F. Pérez-Guevara, P.D. Roy, G. Kutralam-Muniasamy, Analyzing microplastics with Nile Red: Emerging trends, challenges, and prospects, J. Hazard. Mater. 423 (Pt B) (2022) 127171.

[21] D.I. Danylchuk, S. Moon, K.e. Xu, A.S. Klymchenko, Switchable Solvatochromic Probes for Live-Cell Super-resolution Imaging of Plasma Membrane Organization, Angew. Chem. Int. Ed. Engl. 58 (42) (2019) 14920–14924.

[22] D.I. Danylchuk, P.-H. Jourard, A.S. Klymchenko, Targeted Solvatochromic Fluorescent Probes for Imaging Lipid Order in Organelles under Oxidative and Mechanical Stress, J. Am. Chem. Soc. 143 (2) (2021) 912–924.

[23] V. Martinez, M. Henary, Nile Red and Nile Blue: Applications and Syntheses of Structural Analogues, Chemistry 22 (2016) 13764–13782.

[24] C.A. Guido, B. Mennucci, D. Jacqueminc, C. Adamo, Planar vs. twisted intramolecular charge transfer mechanism in Nile Red: new hints from theory, PCCP 12 (2010) 8016–8023.

[25] F.M. Goñi, A. Alonso, L.A. Bagatolli, R.E. Brown, D. Marsh, M. Prieto, J.L. Thewalt, Phase diagrams of lipid mixtures relevant to the study of membrane rafts, BBA 1781 (11-12) (2008) 665–684.

[26] M. Ibarguren, A. Alonso, B.G. Tenchov, F.M. Goñi, Quantitation of cholesterol incorporation into extruded lipid bilayers, BBA 1798 (9) (2010) 1735–1738.

[27] R. Siavashi, T. Phaterpekar, S.S.W. Leung, A. Alonso, F.M. Goñi, J.L. Thewalt, Lamellar Phases Composed of Phospholipid, Cholesterol, and Ceramide, as Studied by 2H NMR, Biophys. J. 117 (2) (2019) 296–306.

[28] A. Keyvanloo, M. Shaghaghi, M.J. Zuckermann, J.L. Thewalt, The Phase Behavior and Organization of Sphingomyelin/Cholesterol Membranes: A Deuterium NMR Study, Biophys. J. 114 (2018) 1344–1356.

[29] R.L. Biltonen, D. Lichtenberg, The use of differential scanning calorimetry as a tool to characterize liposome preparations, Chem. Phys. Lipids 64 (1993) 129–142.

[30] J.A. Levitt, P.H. Chung, K. Suhling, Spectrally resolved fluorescence lifetime imaging of Nile red for measurements of intracellular polarity, J. Biomed. Opt. 20 (2015) 096002.

[31] G. Weber, Polarization of the fluorescence of macromolecules. I. Theory and experimental method, Biochem. J. 51 (1952) 145–155.

[32] M. Levitus, Handbook of Fluorescence Spectroscopy and Imaging. From Ensemble to Single Molecules. Edited by Markus Sauer, Johan Hofkens and Jörg Enderlein., Angew. Chem. Int. Ed. 50 (39) (2011) 9017–9018.

[33] C.Y. Cheng, L.L.C. Olijve, R. Kausik, S. Han, Cholesterol enhances surface water diffusion of phospholipid bilayers, J. Chem. Phys. 141 (2014) 22D513.

[34] M.I. Angelova, D.S. Dimitrov, Liposome electroformation, Faraday Discuss. Chem. Soc. 81 (1986) 303–311.

[35] D.S. Dimitrov, M.I. Angelova, Lipid swelling and liposome formation mediated by electric fields, Bioelectrochem Bioenerg. 19 (2) (1988) 323–336.

[36] M. Fidorra, L. Duelund, C. Leidy, A.C. Simonsen, L.A. Bagatolli, Absence of fluid-ordered/fluid-disordered phase coexistence in ceramide/POPC mixtures containing cholesterol, Biophys. J. 90 (12) (2006) 4437–4451.